Anti-Unwinding Attitude Control of Spacecraft with Forbidden Pointing Constraints

Qinglei Hu* and Biru Chi†
Beihang University, 100191 Beijing, People's Republic of China
and
Maruthi R. Akella‡
University of Texas at Austin, Austin, Texas 78712-1221

DOI: 10.2514/1.G003606

A new algorithm is proposed for rigid spacecraft attitude reorientation guidance under forbidden pointing constraints. Specifically, in view of the parameterized forbidden orientations using the unit quaternion, a special potential function is formulated for spacecraft guidance to ensure that the attitude converges to the desired attitude while avoiding pointing toward the forbidden orientations. Based on the explicit incorporation of an anti-unwinding attitude error function as a component of this potential function, the redundancy that is naturally associated with the quaternion representation is shown to have no adverse impact upon convergence to the global minima. Saliently, the unwinding phenomenon allows for automatically choosing the closer equilibrium. Analysis is performed to establish the existence of the potential field's critical points, and a solution is given to avoid them for any given initial configuration. Numerical simulations are performed to illustrate the effectiveness and performance of the proposed algorithm.

I. Introduction

DIVERSE and complex mission requirements are increasingly being imposed upon on-orbit spacecraft reorientation functions with rapid development of autonomous missions involving space robotics. Inside the space environment, some undesirable objects have potential adverse impacts during spacecraft reorientation missions, by virtue of the requirements of onboard sensitive payload, such as infrared telescopes or star sensor, whose boresights should be pointed away from the direct exposure of bright objects. Hence, the requirement of the boresight's evasion introduces the notion of attitude forbidden constraint (AFC). Spacecraft attitude reorientation subject to AFC is a significant challenge not only from a practical perspective, but it also brings major theoretical difficulties for the attitude controller design due to the barriers arising from the noncontractible configuration space of attitude motion.

Several guidance-based solutions have been proposed for spacecraft reorientation problems in previous literature, such as adaptive control [1], sliding-mode control [2,3], optimal control [4], and predictive control [5]. However, the problem of AFC is typically not explicitly taken into consideration in much of the classical literature. Spacecraft reorientation problems under attitude constraints have been addressed in a few relatively recent papers, and the corresponding solutions could be generally divided into two categories: path planning methods and artificial potential function (APF) methods [6,7]. The first approach aims to design a predetermined permissible trajectory toward avoiding the unwanted orientations. Spindler [8] proposed a cost function to penalize both high angular velocities and the attitudes close to the forbidden direction, and then optimal control solutions were introduced to determine a suitable control law. Hablani [9] took advantage of geometric relations to determine a motion planning with all the attitude requirements satisfied. Cui et al. [10] and Frazzoli et al. [11] solved the AFC problem using randomized motion planning methods, but a knotty problem emerged for the fact that the computational time increases with growing number of attitude constraints. Kjellberg and Lightsey [12] used the A^* pathfinding algorithm to find an optimal path away from the forbidden zones by discretizing the unit quaternion into graphs. Building on the work of [12], Tanygin [13] discretized the possible maneuver attitudes in a three-dimensional projected space and employed the graph search algorithm to find the shortest constrained path. The model predictive control (MPC) method [14] was also applied to solve the constrained attitude problem by using the exterior penalty function to handle the control constraints and attitude constraints.

The path planning method has been widely studied for its effectiveness to solve AFC issues; however, its implementation for real-time settings is often rather complicated [15], and an alternative approach is the APF method [6,7,15–20] with several applications in the robotics area. Power function with negative base [6,7], logarithm function [15,16], Gaussian function [17], and exponential function [18] have all been adopted for the purpose of designing the repulsive potential function. Wisniewski and Kulczycki [19] defined two orthonormal vectors and formulated a novel APF to avoid the onboard camera's exposure to the sun. Mengali and Quarta [20] introduced discrete/continuous control laws based on a switching APF to keep spacecraft satisfying the constraints during orientation. However, an intractable problem often associated with APF methods is the existence of critical points (resulted by the balance of attractive and repulsive forces), including local minima and saddle points. Much of the aforementioned literature does not take these critical points into consideration to our best knowledge. The critical points may adversely influence the convergence of the system and drive the states deviating from the desired equilibria. In view of this limitation, the implementation discussed in [16,21] aims to break the symmetry condition of saddle points. Doria et al. [22] applied the deterministic annealing approach to avoid the robot from getting trapped in a local minimum. In Ref. [23], the robot agents were prevented from being trapped in local minima by forcing them to exit from the region where local minima may exist.

Another practical problem is the unwinding phenomenon caused by the redundancy of attitude representation, such as the unit quaternion. With respect to the unit quaternion's definition [24–26], the spacecraft attitude can be parameterized by two antipodal unit quaternions (in the quaternion setting, both $\boldsymbol{Q}$ and $-\boldsymbol{Q}$ represent the same physical orientation), such that the quaternion-based attitude

Received 29 January 2018; revision received 24 August 2018; accepted for publication 7 September 2018; published online 29 November 2018.

*Professor, School of Automation Science and Electrical Engineering; huql_buaa@buaa.edu.cn. Associate Fellow AIAA (Corresponding Author).

†Graduate Student, School of Automation Science and Electrical Engineering; chibiru@buaa.edu.cn.

‡Professor, E. P. Schoch Endowed Professorship in Engineering, Department of Aerospace Engineering and Engineering Mechanics; makella@mail.utexas.edu. Associate Fellow AIAA.

control system is endowed with two equilibria. However, in most existing literature, only one of the two equilibria is stabilized, and the other is considered unstable, thereby resulting in the unwinding phenomenon (spacecraft tumbles through an unnecessary large rotation) and leading to higher fuel use and longer maneuver durations. Hu et al. [27,28] introduced the anti-unwinding error function and attitude error vectors to address the presence of the two attitude equilibria. Mayhew et al. [29] employed the sign function to avoid the unwinding motion and introduced a hysteresis mechanism to prevent the undesired switch triggered by measurement errors. An anti-unwinding sliding surface was applied to ensure the attitude stabilization in [30].

In this work, a new potential function is constructed to specifically handle the spacecraft reorientation problem subject to forbidden constraints. The forbidden zones are described in view of geometric relations using the unit quaternions, and correspondingly quadratic forbidden constraints are formulated. With the anti-unwinding requirement explicitly taken into consideration, the new APF presented here naturally incorporates the anti-unwinding attitude error function, which guarantees that both the ordinary equilibrium quaternion and its redundant counterpart quaternion are global minimizers. Further analysis establishes the existence and explicit characterization of the potential field's critical points, which are uniquely determined by the APF's parameters. Furthermore, a model-independent APF-based controller is presented to guide the spacecraft motion toward the target orientation along a closer path (i.e., no unwinding) and avoid all the forbidden constraints during the reorientation. The proposed attitude control scheme is shown to result in asymptotic convergence of the error states. The algorithm provides for spacecraft rotational motion with reaching the desired attitude as represented by the closer equilibrium and no violation of AFC. A nice benefit of this solution is the shortening of maneuver paths, and energy consumption is typically lower compared to the reorientation arriving at the farther equilibrium.

The remainder of this paper is organized as follows. Section II states the attitude control problem for a rigid spacecraft under attitude forbidden constraints, and an anti-unwinding error function is then introduced for the redundancy of quaternion representation. Subsequently, Sec. III presents the main contributions of this work, including the APF design and the asymptotic stability analysis for the closed-loop system. Numerical simulation results are illustrated in Sec. IV to show the effectiveness and performance of the proposed algorithm. Finally, conclusions are made in Sec. V.

II. Preliminaries

In this section, we review the spacecraft attitude dynamics and derive a mathematical representation of AFC. The unit quaternion is adopted to represent the orientation of spacecraft in the body frame $\mathcal{B}$ with respect to the inertial frame $\mathcal{I}$. Given the Euler rotation unit axis $\boldsymbol{e} \in \mathbb{R}^3$ and rotation angle $\psi \in [0, 2\pi]$, the unit quaternion $\boldsymbol{Q} = [\boldsymbol{q}^T, q_0]^T = [\boldsymbol{e}^T \sin(\psi/2), \cos(\psi/2)]^T$ is composed of the vector part $\boldsymbol{q} \in \mathbb{R}^3$ and the scalar part $q_0 \in \mathbb{R}$. Consequently, the unit quaternion $\boldsymbol{Q}$ satisfies the unit-norm constraint $\|\boldsymbol{Q}\|^2 = \boldsymbol{q}^T\boldsymbol{q} + q_0^2 = 1$. Define the set of the unit quaternion as $\mathbb{Q} = \{\boldsymbol{Q} \in \mathbb{R}^3 \times \mathbb{R} | \|\boldsymbol{Q}\| = 1\}$, and the quaternion multiplication is given as

$$\boldsymbol{Q}_a \otimes \boldsymbol{Q}_b = \begin{bmatrix} q_{a0}\boldsymbol{q}_b + q_{b0}\boldsymbol{q}_a + \boldsymbol{q}_a \times \boldsymbol{q}_b \\ q_{a0}q_{b0} - \boldsymbol{q}_a^T\boldsymbol{q}_b \end{bmatrix} \tag{1}$$

where $\boldsymbol{Q}_a = [\boldsymbol{q}_a^T, q_{a0}]^T \in \mathbb{Q}$, and $\boldsymbol{Q}_b = [\boldsymbol{q}_b^T, q_{b0}]^T \in \mathbb{Q}$.

A. Spacecraft Attitude Dynamics

The kinematic and dynamic equations of a rigid spacecraft are given by

$$\dot{\boldsymbol{Q}} = \frac{1}{2}\begin{bmatrix} q_0\boldsymbol{\omega} + \boldsymbol{q}^\times\boldsymbol{\omega} \\ -\boldsymbol{q}^T\boldsymbol{\omega} \end{bmatrix} = \frac{1}{2}\boldsymbol{Q} \otimes \tilde{\boldsymbol{\omega}} \tag{2}$$

$$\boldsymbol{J}\dot{\boldsymbol{\omega}} = -\boldsymbol{\omega}^\times\boldsymbol{J}\boldsymbol{\omega} + \boldsymbol{\tau} \tag{3}$$

where $\boldsymbol{\omega} \in \mathbb{R}^3$ denotes the angular velocity of spacecraft with respect to the inertial frame $\mathcal{I}$; $\tilde{\boldsymbol{\omega}} \in \mathbb{R}^3 \times \mathbb{R}$ is defined as $\tilde{\boldsymbol{\omega}} = [\boldsymbol{\omega}^T, 0]^T$; $\boldsymbol{J} = \boldsymbol{J}^T \in \mathbb{R}^{3\times3}$ is the positive-definite inertia matrix of the spacecraft; $\boldsymbol{\tau} \in \mathbb{R}^3$ represents the external control torque; and $\boldsymbol{q}^\times$ denotes a skew-symmetric matrix of the vector $\boldsymbol{q} = [q_1, q_2, q_3]^T$, such that

$$\boldsymbol{q}^\times = \begin{bmatrix} 0 & -q_3 & q_2 \\ q_3 & 0 & -q_1 \\ -q_2 & q_1 & 0 \end{bmatrix}$$

Given the desired attitude $\boldsymbol{Q}_d = [\boldsymbol{q}_d^T, q_{d0}]^T \in \mathbb{Q}$ and its conjugate $\boldsymbol{Q}_d^* = [-\boldsymbol{q}_d^T, q_{d0}]^T \in \mathbb{Q}$, the error quaternion between $\boldsymbol{Q}$ and $\boldsymbol{Q}_d$ is defined as

$$\begin{aligned} \boldsymbol{Q}_e = [\boldsymbol{q}_e^T, q_{e0}]^T = \boldsymbol{Q}_d^* \otimes \boldsymbol{Q} &= \begin{bmatrix} q_{d0}\boldsymbol{q} - q_0\boldsymbol{q}_d - \boldsymbol{q}_d \times \boldsymbol{q} \\ q_{d0}q_0 + \boldsymbol{q}_d^T\boldsymbol{q} \end{bmatrix} \\ &= \begin{bmatrix} \sin\dfrac{\psi_e}{2}\boldsymbol{e}_e^T, \cos\dfrac{\psi_e}{2} \end{bmatrix}^T \end{aligned} \tag{4}$$

where $\boldsymbol{e}_e$ is the rotation axis, and ψ_e is the rotation angle. The attitude error kinematics is given by

$$\dot{\boldsymbol{Q}}_e = \frac{1}{2}\boldsymbol{Q}_e \otimes \tilde{\boldsymbol{\omega}} = \frac{1}{2}\begin{bmatrix} q_{e0}\boldsymbol{\omega} + \boldsymbol{q}_e^\times\boldsymbol{\omega} \\ -\boldsymbol{q}_e^T\boldsymbol{\omega} \end{bmatrix} \tag{5}$$

B. Attitude Forbidden Constraints

Suppose that the unit vector $\boldsymbol{n}_b^B$ in the body frame $\mathcal{B}$ is the boresight vector of the sensitive instrument (such as infrared telescope) onboard, and the unit forbidden vector $\boldsymbol{n}_o^I$ points toward the obstacle (such as sun) from spacecraft's center in the inertial frame $\mathcal{I}$, as shown in Fig. 1. During the reorientation, a minimum keep-out angle θ_m must be maintained for the safety of the instrument, which means the instantaneous angle θ between the boresight vector and the forbidden vector must be greater than θ_m:

$$\theta > \theta_m \tag{6}$$

where $\boldsymbol{n}_b^I = \boldsymbol{C}(\boldsymbol{Q})^T\boldsymbol{n}_b^B$ is the expression of $\boldsymbol{n}_b^B$ in the inertia frame $\mathcal{I}$, and $\boldsymbol{C}(\boldsymbol{Q})$ denotes the rotation matrix represented by $\boldsymbol{Q}$ and is given by $\boldsymbol{C}(\boldsymbol{Q}) = (q_0^2 - \boldsymbol{q}^T\boldsymbol{q})I_3 + 2\boldsymbol{q}\boldsymbol{q}^T - 2q_0\boldsymbol{q}^\times$. Generally, the condition in Eq. (6) can be described as

$$\boldsymbol{n}_o^I \cdot \boldsymbol{n}_b^I = \cos\theta < \cos\theta_m \tag{7}$$

Substituting $\boldsymbol{C}(\boldsymbol{Q})$ into Eq. (7) yields

$$(q_0^2 - \boldsymbol{q}^T\boldsymbol{q})(\boldsymbol{n}_o^I)^T\boldsymbol{n}_b^B + 2(\boldsymbol{n}_o^I)^T\boldsymbol{q}\boldsymbol{q}^T\boldsymbol{n}_b^B + 2(\boldsymbol{n}_o^I)^T q_0\boldsymbol{q}^\times\boldsymbol{n}_b^B < \cos\theta_m \tag{8}$$

Then, the preceding inequality can be rewritten as [15]

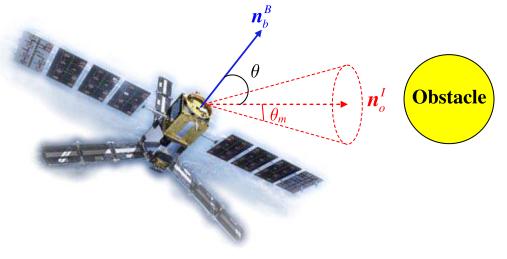

Fig. 1 Attitude forbidden constraint illustration.

$$\boldsymbol{Q}^T\begin{bmatrix}\boldsymbol{n}_o^I(\boldsymbol{n}_b^B)^T+\boldsymbol{n}_b^B(\boldsymbol{n}_o^I)^T-[(\boldsymbol{n}_o^I)^T\boldsymbol{n}_b^B+\cos\theta_m]\boldsymbol{I}_3 & \boldsymbol{n}_b^B\times\boldsymbol{n}_o^I\\ (\boldsymbol{n}_b^B\times\boldsymbol{n}_o^I)^T & (\boldsymbol{n}_o^I)^T\boldsymbol{n}_b^B-\cos\theta_m\end{bmatrix}\boldsymbol{Q}<0 \tag{9}$$

For brevity, let

$$\boldsymbol{M}=\begin{bmatrix}\boldsymbol{n}_o^I(\boldsymbol{n}_b^B)^T+\boldsymbol{n}_b^B(\boldsymbol{n}_o^I)^T-[(\boldsymbol{n}_o^I)^T\boldsymbol{n}_b^B+\cos\theta_m]\boldsymbol{I}_3 & \boldsymbol{n}_b^B\times\boldsymbol{n}_o^I\\ (\boldsymbol{n}_b^B\times\boldsymbol{n}_o^I)^T & (\boldsymbol{n}_o^I)^T\boldsymbol{n}_b^B-\cos\theta_m\end{bmatrix}$$

Then, the inequality in Eq. (9) can be compactly stated through the quadratic constraint

$$\boldsymbol{Q}^T\boldsymbol{M}\boldsymbol{Q}<0 \tag{10}$$

It should be noted that $\boldsymbol{M}$ is symmetric and invertible with the eigenvalues $-1-\cos\theta_m$, $-1-\cos\theta_m$, $1-\cos\theta_m$, and $1-\cos\theta_m$ [15]. Suppose that the total number of sensitive instruments is m, with each instrument having n number of nonoverlapping forbidden zones, and $\boldsymbol{M}_j^i$ denotes the matrix in the jth quadratic constraint for ith sensitive instrument. Thus, the safe orientation attitude outside the forbidden zones can be expressed by the set

$$\mathbb{Q}_s=\{\boldsymbol{Q}\in\mathbb{Q}|\boldsymbol{Q}^T\boldsymbol{M}_j^i\boldsymbol{Q}<0, i=1,\ldots,m, j=1,\ldots,n\} \tag{11}$$

C. Anti-Unwinding Attitude Error Function

Because of the redundancy of the unit quaternion, the attitude motion described by Eqs. (3) and (5) has the two distinct attitude equilibrium points corresponding to $q_{e0}=1$ and $q_{e0}=-1$, both representing the same physical direction [28]. However, in much of the prior literature [31,32], the equilibrium $q_{e0}=1$ is taken to be the only stable point, whereas the other equilibrium $q_{e0}=-1$ is considered unstable. Therefore, the "unwinding" phenomenon might occur (i.e., when the rotation angle ψ_e given in Eq. (4) is greater than π, the trajectory of attitude maneuver is longer, which can lead to the increasing energy consumption and longer maneuver time).

In previous literature [31,32], the term $\boldsymbol{q}_e^T\boldsymbol{q}_e+(1-q_{e0})^2$ acts as the attitude error function to drive the transfer of the state q_{e0} toward 1 and, as a consequence, potentially leads to the unwinding phenomenon. Here, we define a scalar function ϕ to represent the error between the current attitude and the target attitude, and the error vector $\boldsymbol{e}_r\in\mathbb{R}^3$ is defined as $\dot{\phi}=\boldsymbol{e}_r^T\boldsymbol{\omega}$.

A commonly used anti-unwinding attitude error function is [33]

$$\phi_1=2(1-q_{e0}^2) \tag{12}$$

Correspondingly, the error vector $\boldsymbol{e}_{r1}$ is given by

$$\boldsymbol{e}_{r1}=2q_{e0}\boldsymbol{q}_e \tag{13}$$

Plots of the error function ϕ_1 and $\|\boldsymbol{e}_{r1}\|$ with respect to ψ_e are shown in Fig. 2. It can be seen that the norm of error vector $\boldsymbol{e}_{r1}$ is lower when the rotation angle gets close to π, which implies that the magnitude of control law generated by error vector gets smaller at maneuvers of rotation angle larger than $\pi/2$. Thus the attitude convergence rate decreases [28]. In addition, this error function introduces an unstable equilibrium $q_{e0}=0$.

To avoid the shortcoming of the aforementioned error function, another anti-unwinding attitude error function is introduced and given by

$$\phi_2=-\log(q_{e0}^2) \tag{14}$$

$$\boldsymbol{e}_{r2}=\frac{1}{q_{e0}}\boldsymbol{q}_e \tag{15}$$

Note that the error vector in Eq. (15) is in fact the Gibbs vector, defined as $\boldsymbol{\rho}_e=\boldsymbol{e}\tan(\psi_e/2)=(\boldsymbol{q}_e/q_{e0})$ [34]. Accordingly, the curves of ϕ_2 and $\|\boldsymbol{e}_{r2}\|$ are shown in Fig. 3. It can be observed that both ϕ_2 and $\|\boldsymbol{e}_{r2}\|$ are monotonically increasing with increasing rotation angle ψ_e. Though both the error function and the error vector are discontinuous at $q_{e0}=0\,(\psi_e=\pi)$, the controller is continuous on the condition that the initial error q_{e0} is nonzero for the rotation angle within π.

The subset $\mathbb{Q}_p$ composed of the safe orientations and the permissible attitude according to anti-unwinding error function can be written as

$$\mathbb{Q}_p=\{\boldsymbol{Q}\in\mathbb{Q}_s|\boldsymbol{Q}^T\boldsymbol{Q}_d\neq 0\} \tag{16}$$

where the desired attitude $\boldsymbol{Q}_d$ belongs to $\mathbb{Q}_s$.

Remark 1: The proposed attitude error function in Eq. (14) is discontinuous and approaches infinity at $q_{e0}=0\,(\psi_e=\pi)$. With

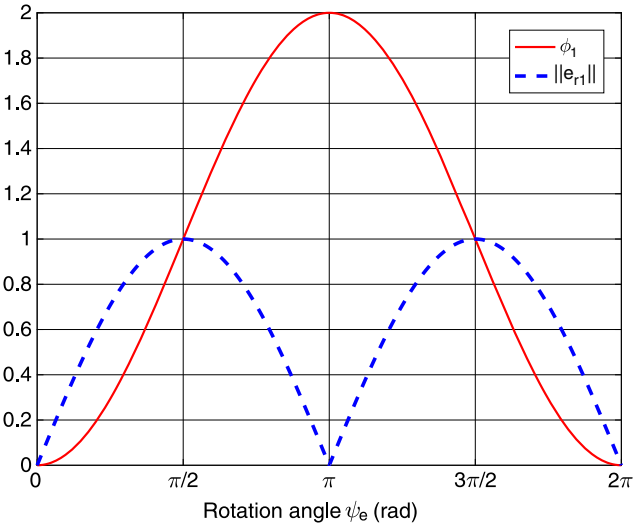

Fig. 2 Curves of ϕ_1 and $\|\boldsymbol{e}_{r1}\|$.

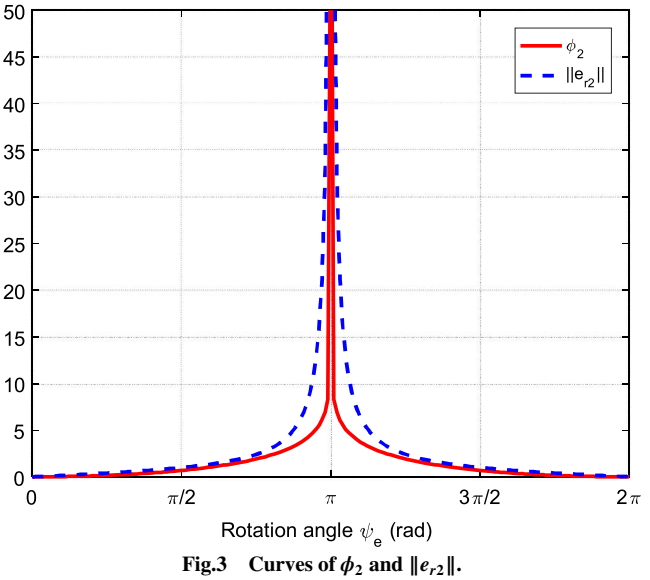

Fig.3 Curves of ϕ_2 and $\|\boldsymbol{e}_{r2}\|$.

this arrangement, the rotation angle of the spacecraft maintains within π during the reorientation, such that the singularity $q_{e0} = 0$ would not be passed during the maneuver process. However, this poses a requirement that the initial q_{e0} does not equal zero exactly.

III. Controller Design

In this section, an APF to handle both attitude forbidden constraints and unwinding phenomenon is presented, and analysis for the potential field shows the existence and location of the critical points. A control law is subsequently proposed to achieve the control objective, and the stability analysis based on Lyapunov theory is performed.

A. Potential Function

A repulsive potential function containing component of the anti-unwinding function is constructed as follows:

$$V_r = \beta\phi_2 \sum_{i=1}^{n}\sum_{j=1}^{m}\frac{-1}{(\boldsymbol{Q}^T\boldsymbol{M}_j^i\boldsymbol{Q})} = \beta\log(q_{e0}^2)\sum_{i=1}^{n}\sum_{j=1}^{m}\frac{1}{(\boldsymbol{Q}^T\boldsymbol{M}_j^i\boldsymbol{Q})} \quad (17)$$

where β is a positive constant. The repulsive potential function in Eq. (17) grows unbounded when the quaternion $\boldsymbol{Q}$ reaches the unsafe attitudes, such as the attitudes that satisfy $\boldsymbol{Q}^T\boldsymbol{M}_j^i\boldsymbol{Q} = 0$ or $\boldsymbol{Q}^T\boldsymbol{Q}_d = 0$. Therefore, as long as V_r remains bounded, the attitude changes in the permissible set $\mathbb{Q}_p$ on condition that the initial attitude belongs to $\mathbb{Q}_p$.

The attractive potential function aims to attract the attitude to the desired equilibrium. One important characteristic of the attractive potential function is that it gets the global minimum at the equilibrium [21]. In this work, we employ the anti-unwinding error function in Eq. (14) as the attractive potential function given by $V_a = \alpha\phi_2 = -\alpha\log(q_{e0}^2)$, where α is a positive constant. Next, the composite potential function is established:

$$V_p = V_a + V_r = -\alpha\log(q_{e0}^2) + \beta\log(q_{e0}^2)\sum_{i=1}^{n}\sum_{j=1}^{m}\frac{1}{(\boldsymbol{Q}^T\boldsymbol{M}_j^i\boldsymbol{Q})} \quad (18)$$

It is obvious that $V_p \geq 0$ for all $\boldsymbol{Q} \in \mathbb{Q}_p$, and $V_p = 0$ only when $\boldsymbol{Q} = \pm\boldsymbol{Q}_d(q_{e0}^2 = 1)$, which guarantees that $\boldsymbol{Q} = \pm\boldsymbol{Q}_d(q_{e0}^2 = 1)$ are global minima.

Take the time derivative of V_p as

$$\dot{V}_p = \nabla V_p^T\dot{\boldsymbol{Q}} \quad (19)$$

where ∇V_p is the gradient of V_p with respect to $\boldsymbol{Q}$, given by

$$\nabla V_p = -\frac{2\alpha}{q_{e0}}\boldsymbol{Q}_d + \frac{2\beta}{q_{e0}}\sum_{i=1}^{n}\sum_{j=1}^{m}\frac{1}{(\boldsymbol{Q}^T\boldsymbol{M}_j^i\boldsymbol{Q})}\boldsymbol{Q}_d - \beta\log(q_{e0}^2)\sum_{i=1}^{n}\sum_{j=1}^{m}\frac{2\boldsymbol{M}_j^i\boldsymbol{Q}}{(\boldsymbol{Q}^T\boldsymbol{M}_j^i\boldsymbol{Q})^2} \quad (20)$$

Substituting Eq. (2) into Eq. (19) yields

$$\dot{V}_p = \frac{1}{2}\nabla V_p^T(\boldsymbol{Q}\otimes\tilde{\boldsymbol{\omega}}) \quad (21)$$

Using the algebraic properties in [15], one has

$$\dot{V}_p = -\frac{1}{2}\tilde{\boldsymbol{\omega}}^T(\nabla V_p^*\otimes\boldsymbol{Q}) = -\frac{1}{2}\boldsymbol{\omega}^T\mathrm{Vec}(\nabla V_p^*\otimes\boldsymbol{Q}) \quad (22)$$

where $\mathrm{Vec}(\cdot)$ denotes the vector parts of the four-element vector $(\cdot)$. Let $\boldsymbol{v} = \mathrm{Vec}(\nabla V_p^*\otimes\boldsymbol{Q})$, where

$$\boldsymbol{v} = -\frac{2\alpha}{q_{e0}}\boldsymbol{q}_e + \frac{2\beta}{q_{e0}}\sum_{i=1}^{n}\sum_{j=1}^{m}\frac{1}{(\boldsymbol{Q}^T\boldsymbol{M}_j^i\boldsymbol{Q})}\boldsymbol{q}_e - 2\beta\log(q_{e0}^2)\sum_{i=1}^{n}\sum_{j=1}^{m}\left\{\frac{1}{(\boldsymbol{Q}^T\boldsymbol{M}_j^i\boldsymbol{Q})^2}\mathrm{Vec}[(\boldsymbol{M}_j^i\boldsymbol{Q})^*\otimes\boldsymbol{Q}]\right\} \quad (23)$$

Proposition 1: The critical points of the APF in Eq. (18) are characterized through the parameters α and β, and the location of the critical points can be changed by adjusting α and β.

Proof: To facilitate subsequent analysis, we define the separation error quaternion $\boldsymbol{Q}_b = [\boldsymbol{q}_b^T, q_{b0}]^T = [\boldsymbol{b}^T\sin(\theta/2), \cos(\theta/2)]^T$ to measure the distance between the instantaneous boresight vector $\boldsymbol{n}_b^B$ and the forbidden vector $\boldsymbol{n}_o^I$, where $\boldsymbol{b} = (\boldsymbol{n}_b^B \times \boldsymbol{n}_o^B/\sin\theta)$ is the related rotation axis, and θ is the rotation angle. The quaternion $\boldsymbol{Q}_b$ reaches $[0, 0, 0, \pm 1]^T$ when the boresight vector $\boldsymbol{n}_b^B$ aligns with $\boldsymbol{n}_o^B$. The kinematics of the separation error quaternion is given by

$$\dot{\boldsymbol{Q}}_b = \frac{1}{2}\boldsymbol{Q}_b\otimes\tilde{\boldsymbol{\omega}} = \frac{1}{2}\begin{bmatrix} q_{b0}\boldsymbol{\omega} + \boldsymbol{q}_b^{\times}\boldsymbol{\omega} \\ -\boldsymbol{q}_b^T\boldsymbol{\omega}\end{bmatrix} \quad (24)$$

Thus, the quadratic constraint in Eq. (10) can be expressed as

$$\boldsymbol{Q}^T\boldsymbol{M}\boldsymbol{Q} = 2q_{b0}^2 - 1 - \cos\theta_m \quad (25)$$

The following discussion about the APF in Eq. (18) is classified by the number of the forbidden attitude constraints. When the orientation is subject to only one forbidden constraint, the APF in Eq. (18) can be written as

$$V_p = \beta\log(q_{e0}^2)\left(\frac{1}{2q_{b0}^2 - 1 - \cos\theta_m} - \frac{\alpha}{\beta}\right) \quad (26)$$

Differentiating V_p in Eq. (26) with respect to time along Eqs. (5) and (24) yields

$$\dot{V}_p = \frac{2\beta}{q_{e0}}\left(\frac{1}{2q_{b0}^2 - 1 - \cos\theta_m} - \frac{\alpha}{\beta}\right)\left(-\frac{1}{2}\boldsymbol{\omega}^T\boldsymbol{q}_e\right) - \frac{4\beta q_{b0}\log(q_{e0}^2)}{(2q_{b0}^2 - 1 - \cos\theta_m)^2}\left(-\frac{1}{2}\boldsymbol{\omega}^T\boldsymbol{q}_b\right) \quad (27)$$

Using rotation axis and angle substituting the quaternion, Eq. (27) is expressed as

$$\dot{V}_p = -\frac{1}{2}\boldsymbol{\omega}^T\left\{2\beta\tan\left(\frac{\psi_e}{2}\right)\left(\frac{1}{\cos\theta - \cos\theta_m} - \frac{\alpha}{\beta}\right)\boldsymbol{e}_e - \frac{2\beta\sin\theta\cdot\log[\cos^2(\psi_e/2)]}{(\cos\theta - \cos\theta_m)^2}\boldsymbol{b}\right\} \quad (28)$$

Thus, the vector $\boldsymbol{v}$ is obtained as

$$\boldsymbol{v} = 2\beta\tan\left(\frac{\psi_e}{2}\right)\left(\frac{1}{\cos\theta - \cos\theta_m} - \frac{\alpha}{\beta}\right)\boldsymbol{e}_e - \frac{2\beta\sin\theta\cdot\log[\cos^2(\psi_e/2)]}{(\cos\theta - \cos\theta_m)^2}\boldsymbol{b} \quad (29)$$

The rotation angle satisfies $\psi_e = 0$ (or 2π) when the spacecraft reaches the desired attitude, corresponding to the condition $\boldsymbol{v} = 0$. However, $\psi_e = 0$ (or 2π) is a sufficient but not necessary condition for $\boldsymbol{v} = 0$. In other words, there exist other solutions to $\boldsymbol{v} = \boldsymbol{0}$ with $\psi_e \neq 0$ (or 2π), and these attitudes are denoted as the critical points of the APF [23]. Using the subscript $\bar{\cdot}$ denoting the corresponding state $\cdot$ at the critical point, $\boldsymbol{v} = \boldsymbol{0}$ and $\psi_e \neq 0$ (or 2π) yields the following condition for critical point:

$$\tan\left(\frac{\bar{\psi}_e}{2}\right)\left(\frac{1}{\cos\bar{\theta} - \cos\theta_m} - \frac{\alpha}{\beta}\right)\bar{\boldsymbol{e}}_e = \frac{\sin\bar{\theta}\cdot\log[\cos^2(\bar{\psi}_e/2)]}{(\cos\bar{\theta} - \cos\theta_m)^2}\bar{\boldsymbol{b}} \quad (30)$$

The critical point requires the vector condition for $\bar{\boldsymbol{e}}_e$ and $\bar{\boldsymbol{b}}$ and the scalar condition for $\bar{\psi}_e$ and $\bar{\theta}$. Here, we assume $\bar{\boldsymbol{e}}_e = \bar{\boldsymbol{b}}$ (without loss of generality because taking $\bar{\boldsymbol{e}}_e = -\bar{\boldsymbol{b}}$ would result in the same final conclusion). The corresponding geometric relation of the various vectors underlying this discussion is shown in Fig. 4. Note that $\boldsymbol{Q}, \boldsymbol{Q}_d$, and $\boldsymbol{Q}_f$ are representing the position of the instantaneous boresight vector, the desired boresight vector, and the forbidden vector on the celestial sphere in the same frame, respectively. Figure 4a shows the geometric interpretation on the celestial sphere. Figures 4b–4d show the direction of the boresight vector's movement in the three plane relations among the boresight vector, the desired position, and the forbidden vector [23]. For the sake of algebraic convenience, the angles ψ_e and θ are assumed to be clockwise started from $\boldsymbol{Q}$. The angle between the desired boresight vector and the forbidden vector is noted as θ_0. The relations between ψ_e and θ in the three scenarios are given by

$$\theta = \psi_e + \theta_0 - 2\pi, \qquad \psi_e \in (2\pi - \theta_0 + \theta_m, 2\pi) \tag{31}$$

$$\theta = \psi_e + \theta_0, \qquad \psi_e \in (\pi, 2\pi - \theta_0 - \theta_m) \tag{32}$$

$$\theta = \psi_e + \theta_0, \qquad \psi_e \in (0, \pi) \tag{33}$$

Substituting Eqs. (31–33) into Eq. (30), we found that Eq. (30) is established only under the geometric relation in Eq. (32), which implies that the critical point only exists under Eq. (32). The scalar condition of critical point is expressed as

$$\frac{\alpha}{\beta} = \frac{1}{\cos\bar{\theta} - \cos\theta_m} - \frac{\sin\bar{\theta} \cdot \log[\cos^2(\bar{\psi}_e/2)]}{(\cos\bar{\theta} - \cos\theta_m)^2 \tan(\bar{\psi}_e/2)} \tag{34}$$

Substituting Eq. (32) into Eq. (34) yields

$$\frac{\alpha}{\beta} = \frac{1}{\cos(\bar{\psi}_e + \theta_0) - \cos\theta_m} - \frac{\sin(\bar{\psi}_e + \theta_0) \cdot \log[\cos^2(\bar{\psi}_e/2)]}{(\cos(\bar{\psi}_e + \theta_0) - \cos\theta_m)^2 \tan(\bar{\psi}_e/2)} \tag{35}$$

It is noted that α/β is monotonically increasing with $\bar{\psi}_e$ in Eq. (35); as a consequence, an increasing α/β yields a larger $\bar{\psi}_e$ and $\bar{\theta}$. Then, we can obtain the critical point's potential value as follows:

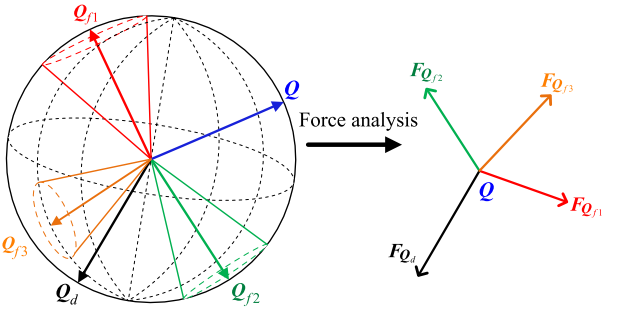

Fig. 5 Geometric relation under multiple forbidden zones.

$$\bar{V}_p = \frac{\beta \log^2[\cos^2(\bar{\psi}_e/2)]\cos(\bar{\psi}_e + \theta_0)}{[\cos(\bar{\psi}_e + \theta_0) - \cos\theta_m]^2} \tag{36}$$

with $\bar{\psi}_e$ increasing, $\bar{V}_p$ is increasing (while keeping β fixed). Thus, increasing α with fixed β would lead to increasing $\bar{\psi}_e, \bar{\theta}$, and $\bar{V}_p$. The location of the critical point can be uniquely determined for a specified value of the ratio α/β. In addition, it is seen that the critical point is closer to the forbidden zone with α/β growing, and its potential value $V_p(\bar{\boldsymbol{Q}})$ increases (with a fixed β).

However, for the situation with multiple attitude constraints, replication of all the preceding steps gets algebraically heavy. Figure 5 shows the spatial relation of the instantaneous boresight vector, the desired vector, and the forbidden vectors in the setting of multiple attitude constraints.

The vector $\boldsymbol{v}$ under multiple AFCs is given by

$$\boldsymbol{v} = 2\beta \boldsymbol{e}_e \tan\left(\frac{\psi_e}{2}\right)\left(\sum_{i=1}^{m}\sum_{j=1}^{n}\frac{1}{\cos\theta_j^i - \cos\theta_{jm}^i} - \frac{\alpha}{\beta}\right) - 2\beta \log\left(\cos^2\frac{\psi_e}{2}\right)\sum_{i=1}^{m}\sum_{j=1}^{n}\frac{\boldsymbol{b}_j^i \sin\theta_j^i}{(\cos\theta_j^i - \cos\theta_{jm}^i)^2} \tag{37}$$

Then, the critical point ($\boldsymbol{v} = \boldsymbol{0}$ but $\psi_e \neq 0$ or 2π) satisfies

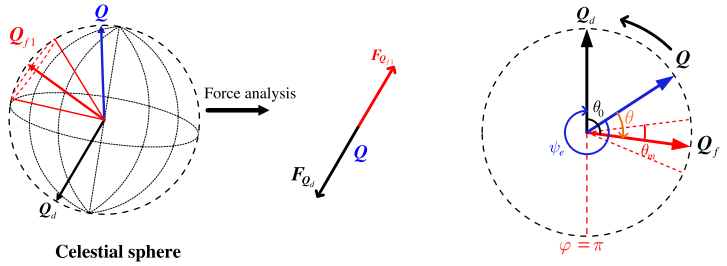

a) Geometric relation on celestial sphere

b) The relation on plane when $\psi_e - \theta = 2\pi - \theta_0$

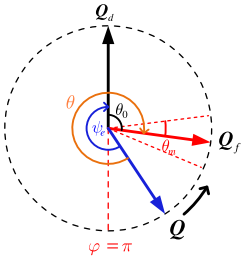

c) The relation on plane when $\psi_e = \theta - \theta_0$ ($\psi_e > \pi$)

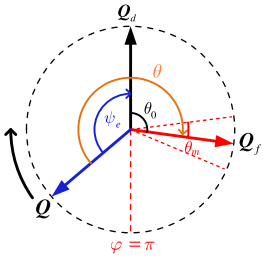

d) The relation on plane when $\psi_e = \theta - \theta_0$ ($\psi_e < \pi$)

Fig. 4 Geometric relations of the rotation.

$$\bar{\boldsymbol{e}}_e \tan\left(\frac{\bar{\psi}_e}{2}\right)\left(\sum_{i=1}^{m}\sum_{j=1}^{n}\frac{1}{\cos\bar{\theta}_j^i-\cos\theta_{jm}^i}-\frac{\alpha}{\beta}\right) = \log\left(\cos^2\frac{\bar{\psi}_e}{2}\right)\sum_{i=1}^{m}\sum_{j=1}^{n}\frac{\bar{\boldsymbol{b}}_j^i\sin\bar{\theta}_j^i}{(\cos\bar{\theta}_j^i-\cos\theta_{jm}^i)^2} \tag{38}$$

The high and low corner mark denotes the ith sensitive instrument and jth forbidden constraint, respectively. Under multiple AFCs, the vector condition of critical point is $\bar{\boldsymbol{e}}_e$, collinear with the vector

$$\sum_{i=1}^{m}\sum_{j=1}^{n}\frac{\bar{\boldsymbol{b}}_j^i\sin\bar{\theta}_j^i}{(\cos\bar{\theta}_j^i-\cos\theta_{jm}^i)^2}$$

Multiplying $\bar{\boldsymbol{e}}_e^T$ from left in Eq. (38) yields

$$\frac{\alpha}{\beta}=\sum_{i=1}^{m}\sum_{j=1}^{n}\frac{1}{(\cos\bar{\theta}_j^i-\cos\theta_{jm}^i)} -\frac{\log(\cos^2(\bar{\psi}_e/2))}{\tan(\bar{\psi}_e/2)}\sum_{i=1}^{m}\sum_{j=1}^{n}\frac{\bar{\boldsymbol{e}}_e T\bar{\boldsymbol{b}}_j^i\sin\bar{\theta}_j^i}{(\cos\bar{\theta}_j^i-\cos\theta_{jm}^i)^2} \tag{39}$$

Once again, it can be observed that α/β determines the location of the critical points. Notice that the number of the critical points may increase with the number of AFC increasing. Changing α/β (such as increasing α while keeping β fixed) would change the value of $\bar{\psi}_e$ and $\bar{\theta}_j^i$, and correspondingly the locations of the critical points are moved.

In view that the rotation axis $\boldsymbol{b}_j^i$ is defined as

$$\boldsymbol{b}_j^i=\frac{\boldsymbol{n}_b^{Bi\times}\boldsymbol{n}_{oj}^{Bi}}{\sin\theta_j^i}$$

one has

$$\bar{\boldsymbol{e}}_e^T\bar{\boldsymbol{b}}_j^i=\frac{\bar{\boldsymbol{e}}_e^T(\bar{\boldsymbol{n}}_b^{Bi\times}\boldsymbol{n}_{oi}^{Bi})}{\sin\bar{\theta}_j^i} \tag{40}$$

Then, the potential value of the critical point is given by

$$\bar{V}_p=\frac{\beta\log^2[\cos^2(\bar{\psi}_e/2)]}{\tan(\bar{\psi}_e/2)}\sum_{i=1}^{m}\sum_{j=1}^{n}\frac{\bar{\boldsymbol{e}}_e^T(\bar{\boldsymbol{n}}_b^{Bi}\times\boldsymbol{n}_{oj}^{Bi})}{(\cos\bar{\theta}_j^i-\cos\theta_m)^2} \tag{41}$$

with the location of the critical point moving due to the change in value of ratio α/β, and the potential value of critical point $\bar{V}_p$ is correspondingly changed.

As a result, the potential function $V_p(\boldsymbol{Q})$ in Eq. (18) has the set of nondegenerate critical points given in the set

$$E=\{\boldsymbol{Q}\in\mathbb{Q}_p|\boldsymbol{v}(\boldsymbol{Q})=\boldsymbol{0}\}$$

which contains the desired equilibria $\boldsymbol{Q}=\pm\boldsymbol{Q}_d$ ($q_{e0}=\pm1$) and critical points $\bar{\boldsymbol{Q}}$.

Remark 2: The unwinding problem is addressed in $\|\boldsymbol{Q}_e\pm\boldsymbol{Q}_I\|^2$ [15] by choosing the error function as with $\boldsymbol{Q}_I=[0,0,0,1]^T$, and its sign is determined by the initial attitude error to get the shorter maneuver path. In this work, an anti-unwinding error function is employed as the attractive potential function to guarantee the global minimum of the two equilibria $q_{e0}=\pm1$. The key feature lies in the unbounded potential at $q_{e0}=0$, which divides the scalar of error quaternion into two parts by its sign. Therefore, the attitude would converge to $q_{e0}=1$ with positive initial error quaternion scalar and transfer to $q_{e0}=-1$ with negative initial scalar. This enables the system trajectories to converge to the "closer" equilibrium in an automated fashion without any further adjustments to the control law and ensures the rotation angle to stay within π.

Remark 3: The influence of the critical points of the potential field was not taken into consideration in [15], which may cause the attitude motion to be to be trapped at the critical points, and this specific situation will be further analyzed in Sec. IV.C.

Remark 4: For the situation where the forbidden zones are moving slowly in the inertial frame (qualitatively speaking), the proposed APF method can also be applied by artificially inflating the forbidden angle θ_m to ensure that the maneuver stays away from the forbidden zones.

B. Controller Design

Based on the APF designed in Eq. (18), a model-independent proportional-derivative (PD) like control law is derived to guarantee the convergence while avoiding attitude forbidden zones and the unwinding phenomenon.

Proposition 2: Consider the rigid spacecraft attitude reorientation model described in Eqs. (2) and (3). Given the potential function in Eq. (18), the control law is prescribed as

$$\boldsymbol{\tau}=-l_1\boldsymbol{\omega}+\frac{1}{2}\boldsymbol{v} \tag{42}$$

where $l_1>0$, and $\boldsymbol{v}$ is the potential function related vector described in Eq. (23). The spacecraft attitude is guaranteed to asymptotically converge to $\{\boldsymbol{Q}=\pm\boldsymbol{Q}_d,\boldsymbol{\omega}=\boldsymbol{0}\}$ when the initial attitude $\boldsymbol{Q}_0$ satisfies $V_p(\boldsymbol{Q}_0)<\min\{V_p(\bar{\boldsymbol{Q}})\}$, in which $\bar{\boldsymbol{Q}}$ is the critical point relative to the parameters α and β.

Proof: Consider the following Lyapunov-like function candidate:

$$V(\boldsymbol{Q},\boldsymbol{\omega})=\frac{1}{2}\boldsymbol{\omega}^T\boldsymbol{J}\boldsymbol{\omega}+V_p \tag{43}$$

Notice that $V(\boldsymbol{Q},\boldsymbol{\omega})\geq0$ and $V(\boldsymbol{Q},\boldsymbol{\omega})=0$ if and only if $(\boldsymbol{Q},\boldsymbol{\omega})=(\pm\boldsymbol{Q}_d,\boldsymbol{\omega})$, such that $V(\boldsymbol{Q},\boldsymbol{\omega})$ is a positive-definite function. Differentiating V with respect to time results in

$$\dot{V}=\boldsymbol{\omega}^T\boldsymbol{J}\dot{\boldsymbol{\omega}}+\dot{V}_p \tag{44}$$

Substituting Eqs. (3), (22), and (42) into Eq. (44) yields

$$\dot{V}(\boldsymbol{Q},\boldsymbol{\omega})=\boldsymbol{\omega}^T(-\boldsymbol{\omega}^{\times}\boldsymbol{J}\boldsymbol{\omega}+\boldsymbol{\tau})+\frac{1}{2}\boldsymbol{\omega}^T\boldsymbol{v} =-l_1\boldsymbol{\omega}^T\boldsymbol{\omega}=-l_1\|\boldsymbol{\omega}\|^2\leq0 \tag{45}$$

Notice that $\dot{V}(\boldsymbol{Q},\boldsymbol{\omega})$ is zero only when $\|\boldsymbol{\omega}\|=0$. Thus, $\dot{V}(\boldsymbol{Q},\boldsymbol{\omega})$ is negative-semidefinite along any trajectory of the closed-loop system. For the initial state $(\boldsymbol{Q}_0,\boldsymbol{\omega}_0)$, consider the set

$$\Delta=\{(\boldsymbol{Q},\boldsymbol{\omega})|V(\boldsymbol{Q},\boldsymbol{\omega})<V(\boldsymbol{Q}_0,\boldsymbol{\omega}_0),\boldsymbol{Q}\in\mathbb{Q}_p,\boldsymbol{\omega}\in\mathbb{R}^3\} \tag{46}$$

By LaSalle's invariant set theorem [35,36], the states starting from Δ converge to the largest invariant subset of Ω contained in Δ. Because $\dot{V}\equiv0$ implies that $\boldsymbol{\omega}\equiv\boldsymbol{0}$, from Eq. (3) it makes clear that $\boldsymbol{\tau}=\boldsymbol{0}$ is obtained. Examining the control law in Eq. (42), we have $\boldsymbol{v}=\boldsymbol{0}$. Specific to the rest-to-rest reorientation problem discussed, both the initial and desired angular velocity are zero, and therefore the inequality in Eq. (46) is the same with $V_p(\boldsymbol{Q})<V_p(\boldsymbol{Q}_0)$. Thus, the set Ω is given by

$$\Omega=\{(\boldsymbol{Q},\boldsymbol{\omega})|\boldsymbol{Q}\in E\cap\{\boldsymbol{Q}|V_p(\boldsymbol{Q})<V_p(\boldsymbol{Q}_0)\},\boldsymbol{\omega}\equiv\boldsymbol{0}\} \tag{47}$$

In this case, each of the nondegenerate critical points in the set E is an equilibrium of the closed-loop dynamics. Thus, all solutions of the closed-loop system would converge to one of the equilibria in Ω. When the initial attitude satisfies $V_p(\boldsymbol{Q}_0)<\min\{V_p(\bar{\boldsymbol{Q}})\}$, the attitude would converge to the desired equilibrium $\{\boldsymbol{Q}=\pm\boldsymbol{Q}_d,\boldsymbol{\omega}=0\}$. This completes the proof.

Based on the analysis in previous subsection, the ratio α/β determines the location of the critical points. To enlarge the attraction region of the desired equilibria, one simple yet effective method is to increase the critical points' potential value $V_p(\bar{\boldsymbol{Q}})$. As mentioned in Proposition 1, increasing α (with β fixed) would increase the potential

value of the critical points such that $V_p(\bar{\boldsymbol{Q}}) > V_p(\boldsymbol{Q}_0)$ may be established for most initial configurations.

The control gains l_1, α, and β affect the system's transient performance of reaching the equilibrium. The controller given in Eq. (42) can be somewhat viewed as the combination of a PD-like part and a potential function related part; therefore, l_1 is related with the damping rate and natural frequency of the system, and α and β are related to the natural frequency. Faster convergence of the attitude error and angular velocity can be achieved by increasing α and β or decreasing l_1, while the control torque is increased in turn. Thus, proper selection and tuning of these parameters is necessary to for acceptable performance of the system.

Remark 5: In view of Proposition 2, the trajectories of the closed-loop system converge to the desired equilibrium under the control law in Eq. (42) with most initial configurations. The undesired behavior (the states converge to the critical points) occurs rarely in practice for two reasons. First, the parameters α and β can always be judiciously selected and adopted such that all the expected initial configurations are guaranteed to stay within the attraction region of the desired equilibrium as stated in Proposition 1. In such a setting, the spacecraft cannot be trapped in critical points. Second, because of the inevitable presence of unmodeled dynamics, perturbations, and measurement noise, the condition for critical points usually cannot be exactly maintained. However, in certain rare situations, the control law in Eq. (42) may still possibly drive the states to be trapped at the critical point. The main motivation for the proposed remedial control law is precisely to help extracting from the critical point in the case when the system has been trapped. After exiting from the region near the critical point, the normal control law is reactivated.

Recalling the analysis in Sec. III.B, the system is trapped in the critical point with $\boldsymbol{v} = \boldsymbol{\omega} = \boldsymbol{0}$ and $q_{e0} \neq \pm 1$. Thus, we consider that the system is trapped when $\|\boldsymbol{\omega}\| \leq B_\omega$, $\|\boldsymbol{v}\| \leq B_v$ and $\psi_e \geq B_\psi$, where B_ω and B_v are small positive scalars, and $B_\psi = \bar{\psi}_{em} - \delta$ with the minimum rotation angle $\bar{\psi}_{em}$ in critical points and an arbitrary small positive constant δ (B_ω, B_v, and δ should be chosen such that the chattering caused by unmodeled dynamics, computational/numerical error, or measurement noise is avoided). Then, the remedial control law is given by [21]

$$\boldsymbol{\tau} = \mu \text{sgn}(\boldsymbol{\omega}^T \boldsymbol{q}_e^\times \boldsymbol{a}) \boldsymbol{q}_e^\times \boldsymbol{a} \tag{48}$$

where $\boldsymbol{a}$ is the unit vector, which is noncollinear with the vector $\boldsymbol{q}_e$, and μ is a positive constant. Qualitatively speaking, this scheme aims to apply a small "push" to the spacecraft in the direction orthogonal to $\boldsymbol{q}_e$; therefore, the condition for critical point is broken, and the trajectory exits from the critical point region. When the states satisfy $\|\boldsymbol{\omega}\| > B_\omega$ or $\|\boldsymbol{v}\| > B_v$, the spacecraft exits from the region near the critical point, and the control law is switched to Eq. (42). To avoid the "chattering" cycle, wherein the spacecraft motion repeatedly/perpetually enters and exits from the neighborhood of the same critical point region, the direction of escaping from critical points (i.e., the unit vector $\boldsymbol{a}$) needs to be selected carefully. In accordance to the critical point's Hessian matrix, the critical points are categorized into saddle points and local minima. Because of the fact that the saddle points are unstable [23], the spacecraft motion is easy to exit from the saddle points with a small perturbation, and $\boldsymbol{a}$ is any vector noncollinear with $\boldsymbol{q}_e$. However, for the local minimum, the vector $\boldsymbol{a}$ is chosen in such a way to drive the spacecraft rotation toward a direction pointing away from the forbidden zones. This can be adequately ensured by choosing the tuning parameters B_ω and B_v to be sufficiently large in terms of noise bounds. Overall, this aforementioned remedial control mechanism ensures that trajectories of the closed-loop system converge toward the desired equilibrium for any given initial configuration.

IV. Numerical Simulations

To demonstrate the effectiveness and performance of the proposed attitude control schemes, a series of numerical simulations are conducted in the presence of attitude forbidden constraints. The rigid spacecraft is assumed to be with one sensitive instrument (such as infrared telescope), and its boresight is aligned with the Z axis of the body frame $\mathcal{B}$. With several forbidden zones distributing in the maneuver space without overlap, the spacecraft is required to achieve the reorientation and avoiding its boresight vector entering the forbidden zones. The details of the forbidden zones consisted of the inertial unit forbidden vectors, and angles are given in the later sections. It is noted that both the initial and the desired attitude are outside the forbidden zones, and the maneuver angle cannot be π exactly for generality.

To manifest the anti-unwinding action of the controller and the influence of undesired critical points, the first two groups of simulation are conducted with different sign of initial attitude error quaternion scalar, and then the third group investigates the influence of the critical points. Further, the performance of the proposed control scheme with quaternion and angular velocity measurement noise are introduced in the fourth simulation case. The parameters of the inertia matrix and the initial angular velocity of the spacecraft are selected as $\boldsymbol{J} = \text{diag}(300, 200, 190)$ kg $\cdot$ m^2 and $\boldsymbol{\omega}(0) = [0, 0, 0]^T$ rad/s, respectively, in the simulation.

A. Reorientation with $q_{e0}(0) > 0$

The first case is assuming that the scalar of the initial attitude error quaternion is greater than zero. The information of forbidden zones is given in Table 1, and the initial and desired quaternion are selected as $\boldsymbol{Q}_0 = [-0.73, 0.2, 0.253, 0.6026]^T$ and $\boldsymbol{Q}_d = [0, 0, 0, 1]^T$, respectively. Simulations under the control schemes in Eq. (58) of [15] with $\pm\boldsymbol{Q}_I$ (considered as two controllers), the anti-unwinding PD control scheme with the attitude error function in [28], and the MPC method in [14] are also conducted to show the features and performance of the different methods. The control gains are given in Table 2.

The time histories of the angular velocity, control torque, error quaternion, and quadratic constraints are shown in Fig. 6. It is seen that q_{e0} converges to 1 in this simulation condition, and all the forbidden constraints are not violated, with the corresponding quadratic constraints being negative. As seen in Fig. 6a, a high peak of ω_1 appears at about 55 s, which is caused by the fourth quadratic approaching zero, and a big control torque is needed to avoid the constraint, and this process can also be reflected in the high peak on τ_1 in Fig. 6b.

The comparison results under different controllers are shown in Figs. 7 and 8. Figures 7a and 7b plot the trajectories of boresight vector on the inertial celestial sphere (three-dimensional, 3-D) and its projection (two-dimensional, 2-D), respectively. The "circle" and "cross" denote the desired and initial position of the boresight, respectively. The four semi-transparent cones are the forbidden constraint zones on the celestial sphere. One can see in Fig. 7 that all the trajectories reach the target goals. However, the trajectory under the PD controller gets into FZ2, whereas the remaining controllers satisfy the constraints, and their trajectories are outside of all the forbidden zones. Notice that the trajectory under the controller in [15] ($-\boldsymbol{Q}_I$) is much longer than that of the other controllers in virtue of the unsuitable equilibrium. In addition, the trajectory under the MPC method in [14] is along the boundary of FZ2, whereas the other three trajectories of the potential function methods have a distance from the forbidden zones. This is due to the

Table 1 Forbidden zones

Forbidden zone	Boresight vector	Angle, rad
FZ1	$[0.253, -0.37, -0.894]^T$	0.4363
FZ2	$[0, 0.707, 0.707]^T$	0.6981
FZ3	$[-0.853, 0.436, -0.286]^T$	0.5236
FZ4	$[0.957, -0.256, 0.131]^T$	0.3491

Table 2 Control parameters

Controller	Parameters
Proposed controller	$l_1 = 50, \alpha = 3, \beta = 0.2$
Method in [15] (with $\boldsymbol{Q}_I$)	$\alpha = 50, k_1 = 1.4$
Method in [15] (with $-\boldsymbol{Q}_I$)	$\alpha = 50, k_1 = 1.4$
Anti-unwinding PD controller $\boldsymbol{\tau} = -k_1\boldsymbol{\omega} - k_2\boldsymbol{e}_r$	$k_1 = 50, k_2 = 4$

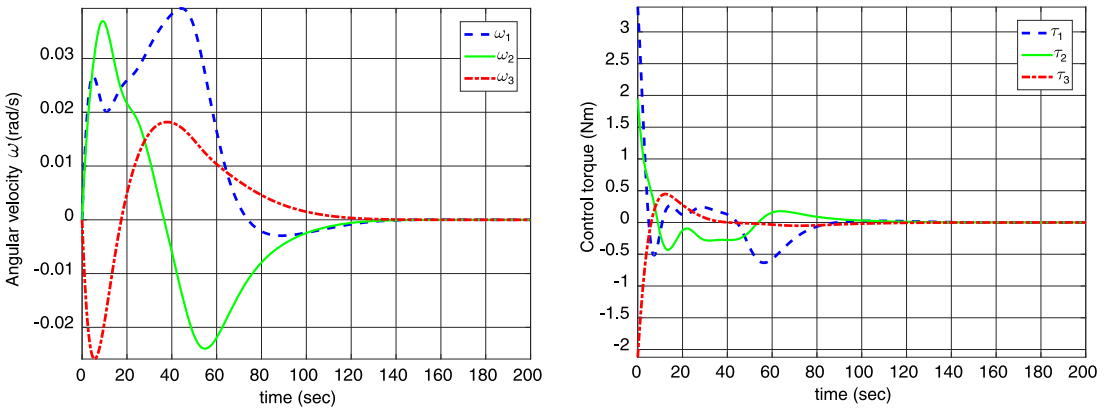

a) Angular velocity ω b) Control torque τ

c) Error quaternion Q_e d) Quadratic constraint $Q^TM_iQ(i=1,2,3,4)$

Fig. 6 Response curves of angular velocity, control torque, error quaternion, and quadratic constraint.

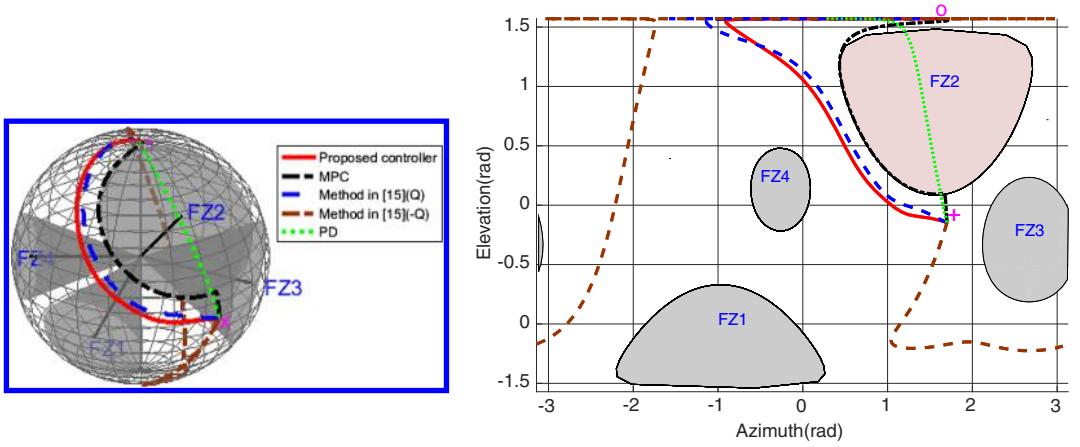

a) Trajectories in 3-D b) Trajectories in 2-D

Fig. 7 Trajectories of sensitive instrument's boresight in 3-D and 2-D.

discontinuity of the penalty function's derivative used in MPC. The penalty function of the MPC method in [14] is similar to the repulsive function that gets high value at the boundary of the forbidden attitudes, whereas it is like a step function such that the function's derivative is discontinuous, and this allows the attitude approaching the boundary.

The norms of error quaternion vector and angular velocity are employed to manifest the attitude error and velocity error, and the energy index defined as

$$\int_0^t \|\boldsymbol{\tau}(t)\|^2 \, \mathrm{d}t$$

is applied to indicate the energy consumed. For a fair comparison, all the methods are tuned to have a similar settling time of attitude and angular velocity error, as shown in Figs. 8a and 8b. In Fig. 8c, the PD controller consumes the least energy, but it fails to satisfy the attitude constraints. The method in [15] ($-\boldsymbol{Q}_I$) has the largest energy consumption for its longer trajectory caused by unwinding phenomenon. In addition, the MPC method's computation is much larger than the potential function methods, as mentioned in Sec. I, which is reflected in the computing time of the simulation.

B. Reorientation with $q_{e0}(0) < 0$

In this subsection, the simulations are conducted with the negative initial error quaternion scalar. The initial and the desired attitude quaternion are $\boldsymbol{Q}_0 = [-0.75, -0.63, 0.18, 0.0906]^T$ and $\boldsymbol{Q}_d = [0.16, 0.8023, -0.1579, 0.553]^T$. Figure 9 plots the response

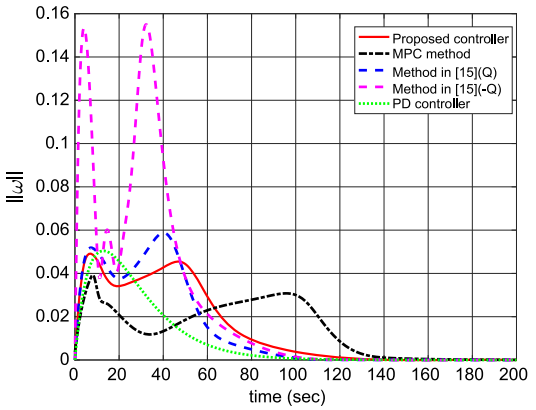

a) Norm of angular velocity

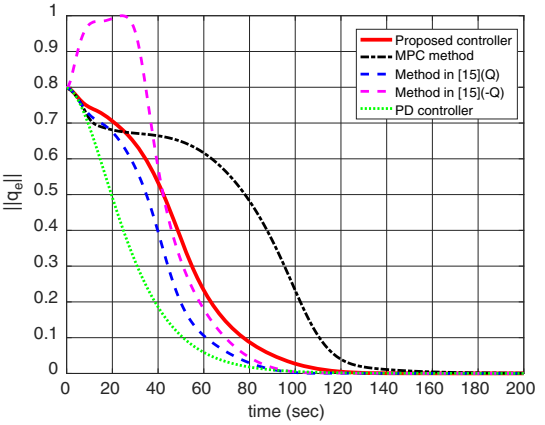

b) Norm of quaternion error

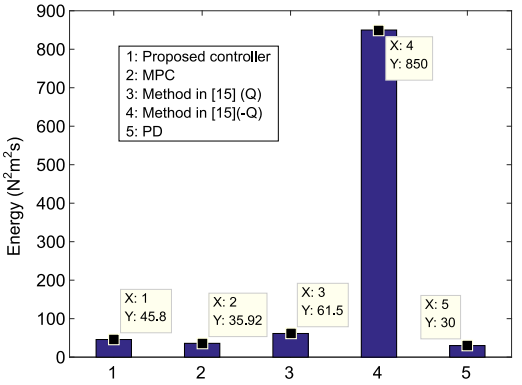

c) Energy consumption

Fig. 8 Simulation results for comparison.

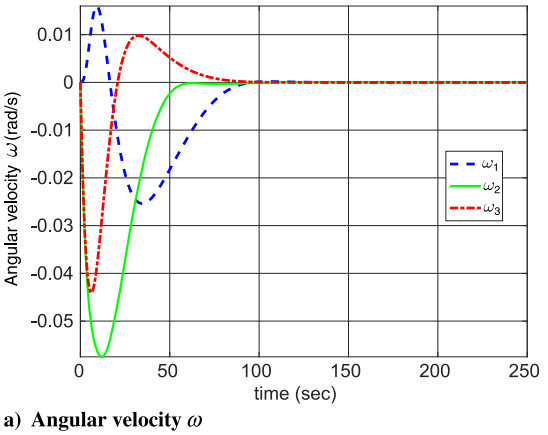

a) Angular velocity ω

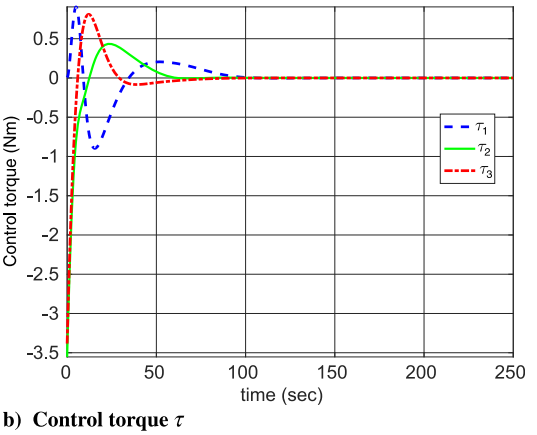

b) Control torque τ

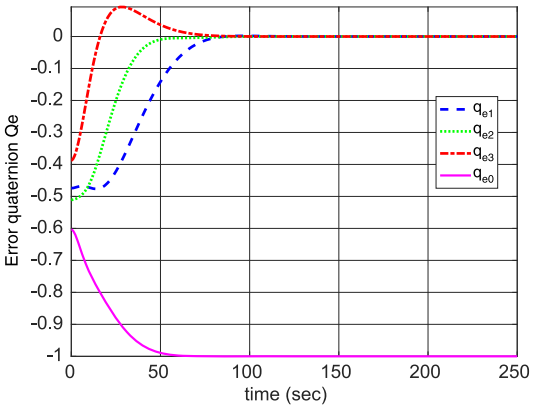

c) Error quaternion Q_e

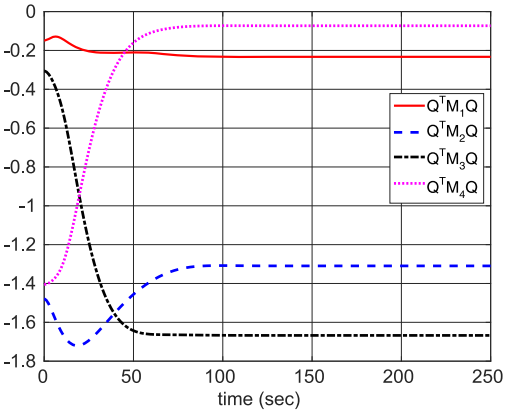

d) Quadratic constraint $Q^T M_i Q (i=1,2,3,4)$

Fig. 9 Simulated time histories of angular velocity, control torque, error quaternion, and quadratic constraint.

curves of the angular velocity, control torque, error quaternion, and quadratic constraints, respectively. In this simulation, q_{e0} converges to -1 with all attitude constraints satisfied.

The trajectories of the boresight onboard under the proposed controller, the method in [15] ($\pm\boldsymbol{Q}_I$), and the PD controller in 3-D and 2-D are figured in Fig. 10. The control parameters follow the condition in Table 2. It can be observed that the controllers based on APF complete the task of avoiding the forbidden zones, whereas the ordinary anti-unwinding PD controller drives the trajectory into the FZ1. In addition, the trajectory of the method in [15] ($\boldsymbol{Q}_I$) is the longest among the trajectories, in contrast to the condition in IV.A. Figures 11a–11c show the comparison results of the attitude error, velocity error, and energy consumption, respectively. As seen, the proposed method and the method in [15] ($-\boldsymbol{Q}_I$) have good performance on the settling time and energy consumption, whereas the method in [15] ($\boldsymbol{Q}_I$) spends a long convergence time and consumes larger energy with negative initial error quaternion scalar.

C. Influence of Critical Point

In practice, the situation when the system is trapped in critical points occurs rarely due to perturbations and measurement noise [16]. However, it also happens when the initial condition is chosen as inappropriate. Thus, the influence of critical point would be discussed in this subsection. For comparison, the simulation under the method in [15] (with $\boldsymbol{Q}_I$) would be performed. The initial attitude $\boldsymbol{Q}_0 = [0.73, 0.2, 0.253, 0.6026]^T$ and the desired attitude $\boldsymbol{Q}_d = [0.9233, 0.3613, -0.1033, -0.0797]^T$ are selected for further simulation. The environment with two forbidden zones is considered, and the control parameters and forbidden zones are given in Table 3.

Figure 12 plots the trajectories under the proposed controller and the method in [15] ($\boldsymbol{Q}_I$), and it shows that proposed controller completes the reorientation and avoids the entry of the forbidden zones. Despite the fact that the trajectory under the method in [15] has no entry of forbidden zones, it stops at critical point and fails to reach

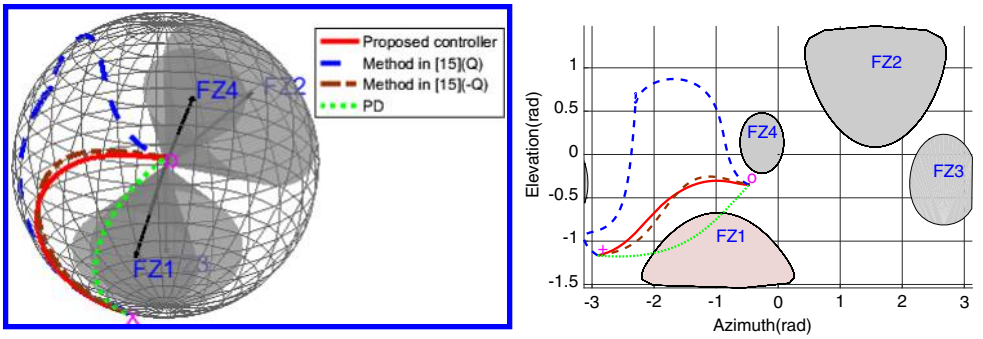

a) Trajectories in 3-D b) Trajectories in 2-D

Fig. 10 Trajectories of sensitive instrument's boresight in 3-D and 2-D.

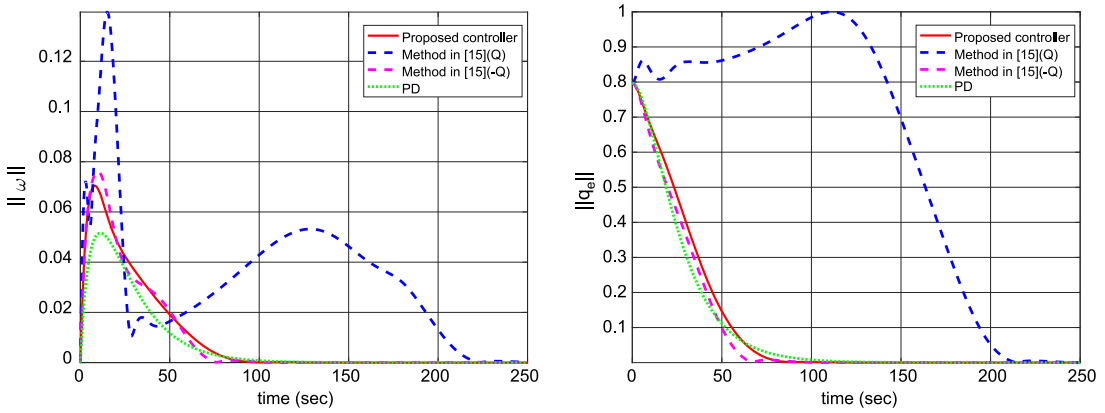

a) Norm of angular velocity b) Norm of quaternion error

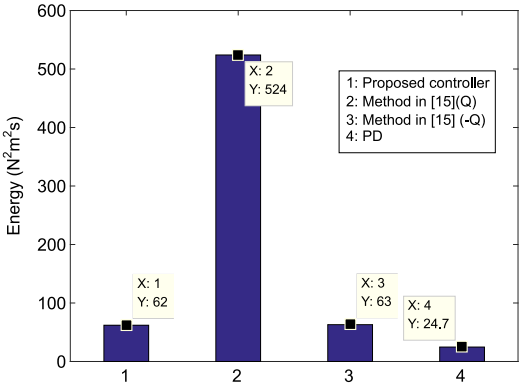

c) Energy consumption

Fig. 11 Simulation results for comparison.

Table 3 Information of the simulation

Forbidden zone	Boresight vector	Angle, rad	Controller	Parameters
FZ1	$[0.253, -0.37, -0.894]^T$	0.4363	Proposed controller	$l_1 = 170, \alpha = 10, \beta = 2$
FZ2	$[-0.433, 0.75, -0.5]^T$	0.5236	Method in [15]	$\alpha = 170, k_1 = 50$

the desired attitude. The time histories of angular velocity, control torque, error quaternion, and quadratic constraints under the two controllers are shown in Figs. 13 and 14, respectively. As shown in Fig. 13, after 160 s, the states $(\boldsymbol{\omega}, \boldsymbol{q}_e)$ converge into $|\omega_i| < 2 \times 10^{-5}$ rad/s and $|q_{ei}| < 1.5 \times 10^{-4}$, $i = 1, 2, 3$. However, the response curves under the method in [15] $(\boldsymbol{Q}_I)$ in Fig. 14 show that the error quaternion stops at $[-0.1146, -0.9585, 0, 0.2613]^T$ after 500 s when $|\omega_i| \leq 2 \times 10^{-4}$ rad/s, and this shows that the system is trapped in the critical point.

D. Performance with Measurement Noise

Next, the simulations under the proposed control scheme in Sec. IV.A are repeated with the measurement noise added to $\boldsymbol{Q}$ and $\boldsymbol{\omega}$, respectively. Using the same approach in [37], the Euler rotation unit axis $\boldsymbol{e}$ is perturbed randomly with the cone angle specified as 0.1 deg. Then, another simulation is conducted in which random noise with mean 0 and variance 10^{-6} is added upon the angular velocity. To illustrate the differences of controller's performance, the norms of angular velocity and the vector part of error quaternion under the

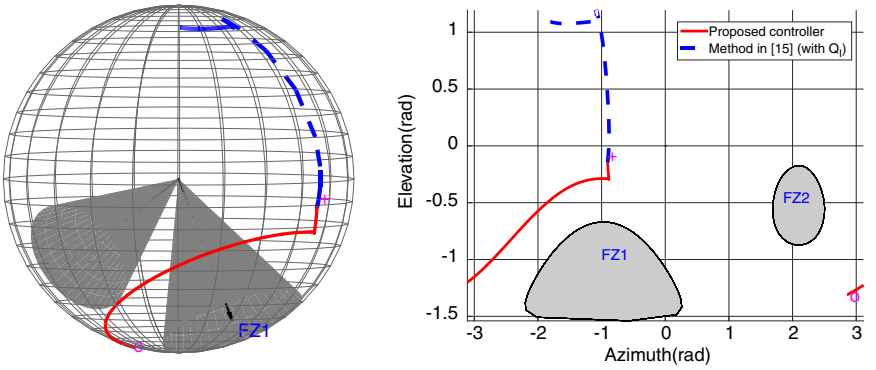

a) Trajectories in 3-D b) Trajectories in 2-D

Fig. 12 Trajectories under different controllers.

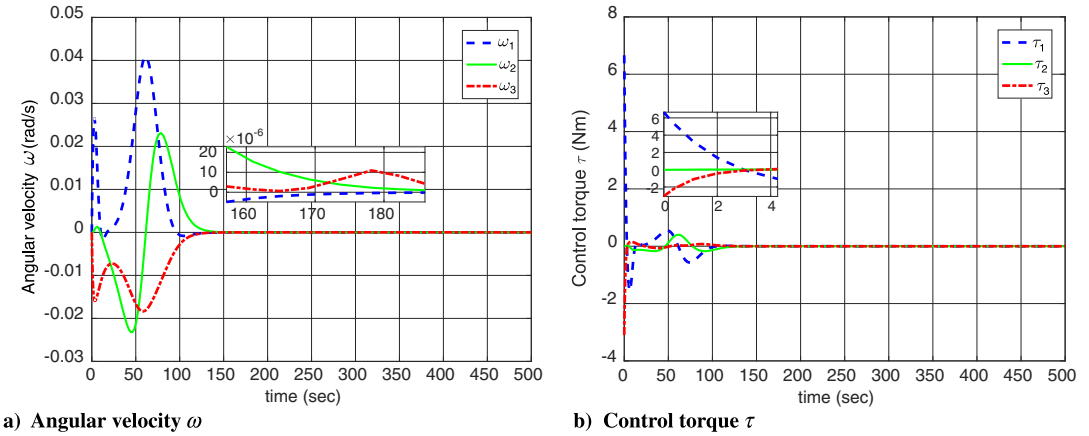

a) Angular velocity ω b) Control torque τ

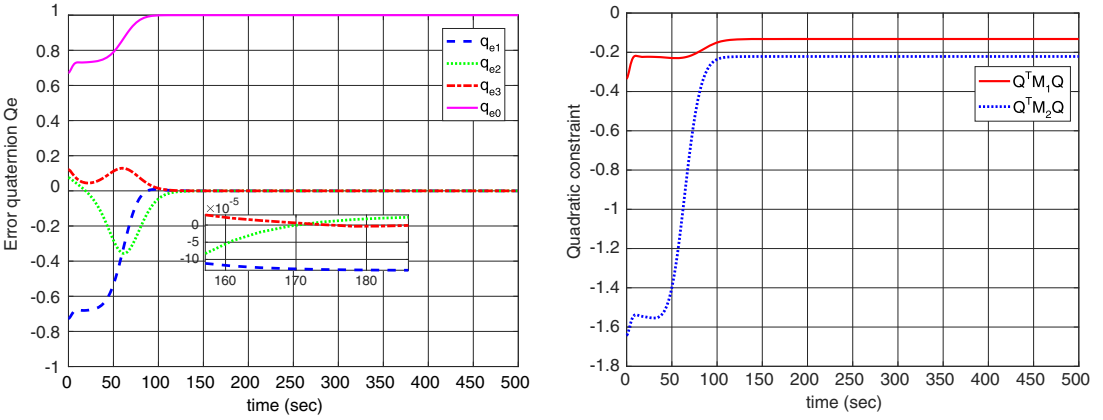

c) Error quaternion Q_e d) Quadratic constraint

Fig. 13 Response curves under the proposed controller.

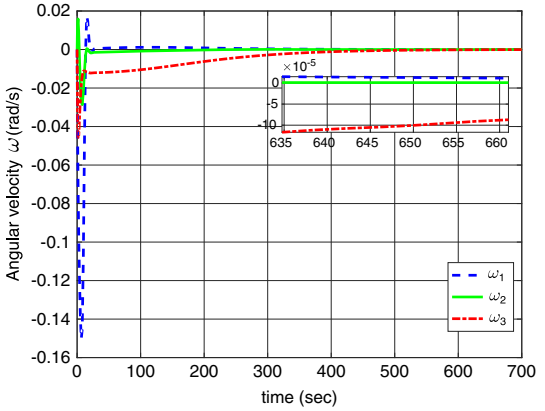

a) Angular velocity ω

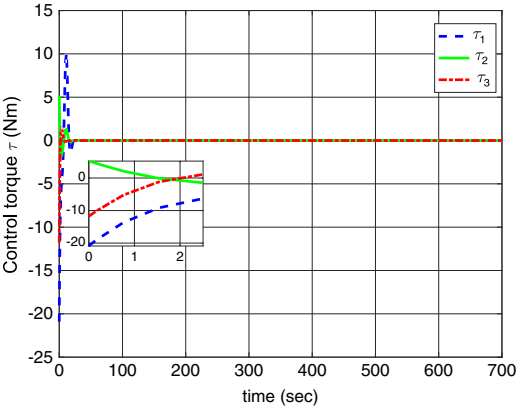

b) Control torque τ

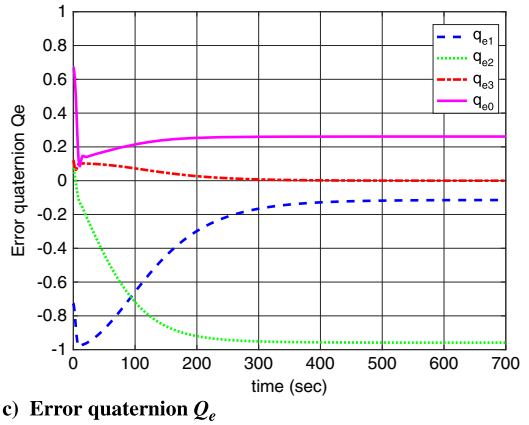

c) Error quaternion Q_e

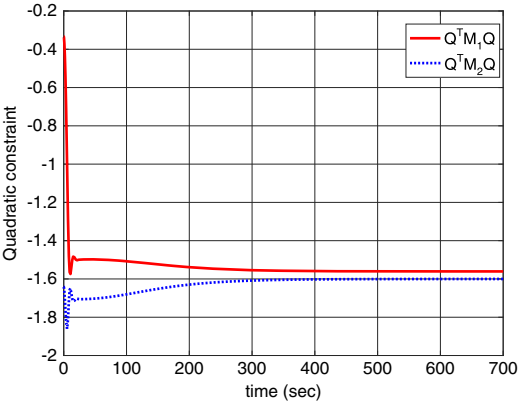

d) Quadratic constraint

Fig. 14 Response curves under the method in [15] (Q_1).

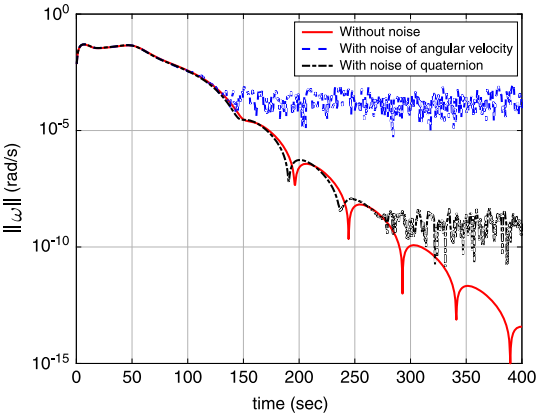

a) Norm of angular velocity

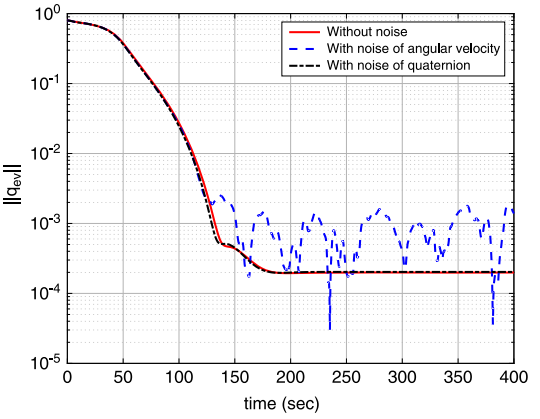

b) Norm of quaternion error

Fig. 15 Performance with measurement noises.

three different conditions are plotted on a semilogarithmic scale in Fig. 15. As expected, it is shown that both the added measurement noises worsen the performance of controller by increasing the steady-state values of the angular velocity and quaternion error.

All the comparison results show that the proposed controller possesses a significant performance for attitude maneuver in the presence of forbidden constraints. It not only completes the requirement of avoiding the forbidden zones but reduces the undesirable effect of unwinding phenomenon.

V. Conclusions

This work focuses on the formulation of guidance laws for spacecraft attitude reorientation in the presence of orientational forbidden constraints and explicit avoidance of the unwinding phenomenon. A special artificial potential function is designed to combine these attitude constraints, and a feedback control law is derived to guarantee the convergence of the closed-loop system without any constraint violation. Extensive numerical simulations confirm and validate the theoretical developments. Further research in this area would focus on the development of the controllers subject to actuator magnitude and rate saturations. In addition, the dynamic attitude constraints with moving forbidden zones would be taken into consideration.

Acknowledgments

This work was supported partially by the National Natural Science Foundation of China (project numbers 61522301 and 61633003). The authors greatly appreciate the financial support. The authors

would also like to thank the associate editor and reviewers for their valuable comments and constructive suggestions that helped to improve the paper significantly.

References

[1] Bošković, J. D., Li, S. M., and Mehra, R. K., "Robust Adaptive Variable Structure Control of Spacecraft Under Control Input Saturation," *Journal of Guidance, Control, and Dynamics*, Vol. 24, No. 1, 2001, pp. 14–22. doi:10.2514/2.4704

[2] Chen, Y. P., and Lo, S. C., "Sliding Mode Controller Design for Spacecraft Attitude Tracking Maneuvers," *IEEE Transaction on Aerospace and Electronics*, Vol. 29, No. 4, 1993, pp. 1328–1333. doi:10.1109/7.259536

[3] Dwyer, T. A. W., III., and Sira-Ramirez, H., "Variable-Structure Control of Spacecraft Attitude Maneuvers," *Journal of Guidance, Control, and Dynamics*, Vol. 11, No. 3, 1988, pp. 262–270. doi:10.2514/3.20303

[4] Lu, P., Cerimele, C., Tigges, M., and Matz, D., "Optimal Aerocapture Guidance," *Journal of Guidance, Control, and Dynamics*, Vol. 38, No. 4, 2015, pp. 553–565. doi:10.2514/1.G000713

[5] Wen, J. T., Seereeram, S., and Bayard, D. S., "Nonlinear Predictive Control Applied to Spacecraft Attitude Control," *Proceedings of the American Control Conference*, IEEE, Piscataway, NJ, 1997, pp. 1899–1903. doi:10.1109/ACC.1997.61

[6] Shen, Q., Yue, C., Goh, C. H., Wu, B., and Wang, D., "Rigid-Body Attitude Stabilization with Attitude and Angular Rate Constraints," *Automatica*, Vol. 90, April 2018, pp. 157–163. doi:10.1016/j.automatica.2017.12.029

[7] Shen, Q., Yue, C. Y., and Goh, C. H., "Velocity-Free Attitude Reorientation of a Flexible Spacecraft with Attitude Constraints," *Journal of Guidance, Control, and Dynamics*, Vol. 40, No. 5, 2017, pp. 1293–1299. doi:10.2514/1.G002129

[8] Spindler, K., "Attitude Maneuvers Which Avoid a Forbidden Direction," *Journal of Dynamical and Control Systems*, Vol. 8, No. 1, 2002, pp. 1–22. doi:10.1023/A:1013907732365

[9] Hablani, H. B., "Attitude Commands Avoiding Bright Objects and Maintaining Communication with Ground Station," *Journal of Guidance, Control, and Dynamics*, Vol. 22, No. 6, 1999, pp. 759–767. doi:10.2514/2.4469

[10] Cui, P., Zhong, W., and Cui, H., "Onboard Spacecraft Slew-Planning by Heuristic State-Space Search and Optimization," *International Conference on Mechatronics and Automation*, IEEE Publ., Piscataway, NJ, 2007, pp. 2115–2119. doi:10.1109/ICMA.2007.4303878

[11] Frazzoli, E., Dahleh, M. A., Feron, E., and Kornfeld, R. P., "A Randomized Attitude Slew Planning Algorithm for Autonomous Spacecraft," *AIAA Guidance, Navigation, and Control Conference and Exhibit*, AIAA Paper 2001-4155, 2001. doi:10.2514/6.2001-4155

[12] Kjellberg, H. C., and Lightsey, E. G., "Discretized Quaternion Constrained Attitude Pathfinding," *Journal of Guidance, Control, and Dynamics*, Vol. 39, No. 3, 2016, pp. 713–718. doi:10.2514/1.G001063

[13] Tanygin, S., "Fast Autonomous Three-Axis Constrained Attitude Pathfinding and Visualization for Boresight Alignment," *Journal of Guidance, Control, and Dynamics*, Vol. 40, No. 2, 2017, pp. 358–370. doi:10.2514/1.G001801

[14] Lee, D., Gupta, R., Kalabić, U., Cairano, S. D., Bloch, A., Cutler, J., and Kolmanovsky, I., "Geometric Mechanics Based Nonlinear Model Predictive Spacecraft Attitude Control with Reaction Wheels," *Journal of Guidance, Control, and Dynamics*, Vol. 40, No. 2, 2017, pp. 309–319. doi:10.2514/1.G001923

[15] Lee, U., and Mesbahi, M., "Feedback Control for Spacecraft Reorientation Under Attitude Constraints via Convex Potentials," *IEEE Transactions on Aerospace and Electronic Systems*, Vol. 50, No. 4, 2014, pp. 2578–2592. doi:10.1109/TAES.2014.120240

[16] Manuel, D. R., and Hanspeter, S., "Kinematic Steering Law for Conically Constrained Torque-Limited Spacecraft Attitude Control," *Journal of Guidance, Control, and Dynamics*, Vol. 41, No. 9, 2018, pp. 1990–2001. doi:10.2514/1.G002873

[17] McInnes, C. R., "Large Angle Slew Maneuvers with Autonomous Sun Vector Avoidance," *Journal of Guidance, Control, and Dynamics*, Vol. 17, No. 4, 1994, pp. 875–877. doi:10.2514/3.21283

[18] Avanzini, G., Radice, G., and Ali, I., "Potential Approach for Constrained Autonomous Maneuvers of a Spacecraft Equipped with a Cluster of Control Moment Gyroscopes," *Proceedings of the Institution of Mechanical Engineers, Part G: Journal of Aerospace Engineering*, Vol. 223, No. 3, 2009, pp. 285–296. doi:10.1243/09544100JAERO375

[19] Wisniewski, R., and Kulczycki, P., "Slew Maneuver Control for Spacecraft Equipped with Star Camera and Reaction Wheels," *Control Engineering Practice*, Vol. 13, No. 3, 2005, pp. 349–356. doi:10.1016/j.conengprac.2003.12.006

[20] Mengali, G., and Quarta, A. A., "Spacecraft Control with Constrained Fast Reorientation and Accurate Pointing," *The Aeronautical Journal*, Vol. 108, No. 1080, 2004, pp. 85–91. doi:10.1017/S0001924000005030

[21] Guo, Y., Li, C., and Ma, G., "Spacecraft Autonomous Attitude Maneuver Control by Potential Function Method," *Acta Aeronautica Et Astronautica Sinica*, Vol. 32, No. 3, 2011, pp. 457–464. doi:CNKI:11.1929/V.20101111.0915.033

[22] Doria, N. S. F., Freire, E. O., and Basilio, J. C., "An Algorithm Inspired by the Deterministic Annealing Approach to Avoid Local Minima in Artificial Potential Fields," *International Conference on Robotics and Automation (ICRA)*, IEEE Publ., Piscataway, NJ, 2013, pp. 1–6. doi:10.1109/ICAR.2013.6766480

[23] Okamoto, M., and Akella, M. R., "Novel Potential-Function-Based Control Scheme for Non-Holonomic Multi-Agent Systems to Prevent the Local Minimum Problem," *International Journal of Systems Science*, Vol. 46, No. 12, 2013, pp. 2150–2164. doi:10.1080/00207721.2013.858795

[24] Joshi, S. M., Kelkar, A. G., and Wen, J. T.-Y., "Robust Attitude Stabilization of Spacecraft Using Nonlinear Quaternion Feedback," *IEEE Transactions on Automatic Control*, Vol. 40, No. 10, 1995, pp. 1800–1803. doi:10.1109/9.467669

[25] Gennaro, S. D., "Passive Attitude Control of Flexible Spacecraft from Quaternion Measurements," *Journal of Optimization Theory and Applications*, Vol. 116, No. 1, 2003, pp. 41–60. doi:10.1023/A:1022106118182

[26] Wie, B., Weiss, H., and Arapostathis, A., ""Quaternion Feedback Regulator for Spacecraft Eigenaxis Rotations," *Journal of Guidance, Control, and Dynamics*, Vol. 12, No. 3, 1989, pp. 375–380. doi:10.2514/3.20418

[27] Hu, Q., Li, L., and Friswell, M. I., "Spacecraft Anti-Unwinding Attitude Control with Actuator Nonlinearities and Velocity Limit," *Journal of Guidance, Control, and Dynamics*, Vol. 38, No. 10, 2015, pp. 2042–2050. doi:10.2514/1.G000980

[28] Hu, Q., and Tan, X., "Unified Attitude Control for Spacecraft under Velocity and Control Constraints," *Aerospace Science and Technology*, Vol. 67, Aug. 2017, pp. 257–264. doi:10.1016/j.ast.2017.04.009

[29] Mayhew, C. G., Sanfelice, R. G., and Teel, A. R., "Quaternion-Based Hybrid Control for Robust Global Attitude Tracking," *IEEE Transactions on Automatic Control*, Vol. 56, No. 11, 2011, pp. 2555–2566. doi:10.1109/TAC.2011.2108490

[30] Tiwari, P. M., Chakraborty, P., and Soni, K. M., "Fault Tolerant Attitude Control Using Anti-Unwinding Second-Order Sliding Mode," *2016 IEEE 1st International Conference on Power Electronics, Intelligent Control and Energy Systems (ICPEICES)*, IEEE Publ., Piscataway, NJ, 2016. doi:10.1109/ICPEICES.2016.7853542

[31] Costic, B. T., Dawson, D. M., de Queiroz, M. S., and Kapila, V., "Quaternion-Based Adaptive Attitude Tracking Controller Without Velocity Measurements," *Journal of Guidance, Control, and Dynamics*, Vol. 24, No. 6, 2001, pp. 1214–1222. doi:10.2514/2.4837

[32] Song, Y. D., and Cai, W., "Quaternion Observer-Based Model-Independent Attitude Tracking Control of Spacecraft," *Journal of Guidance, Control, and Dynamics*, Vol. 32, No. 5, 2009, pp. 1476–1482. doi:10.2514/1.43029

[33] Kristiansen, R., Nicklasson, P. J., and Gravdahl, J. T., "Satellite Attitude Control by Quaternion-Based Backstepping," *IEEE Transactions on Control Systems Technology*, Vol. 17, No. 1, 2009, pp. 227–232. doi:10.1109/TCST.2008.924576

[34] Tsiotras, P., "Stabilization and Optimality Results for the Attitude Control Problem," *Journal of Guidance, Control, and Dynamics*,

Vol. 19, No. 4, 1996, pp. 772–779.
doi:10.2514/3.21698

[35] Sanyal, A., and Chaturvedi, N., "Almost Global Robust Attitude Tracking Control of Spacecraft in Gravity," *AIAA Guidance, Navigation and Control Conference and Exhibit*, AIAA Paper 2008-6979, Aug. 2008.
doi:10.2514/6.2008-6979

[36] Khalil, H. K., *Nonlinear Systems*, Prentice-Hall, Upper Saddle River, NJ, 1996, pp. 113–120.

[37] Akella, M. R., Thakur, D., and Mazenc, F., "Partial Lyapunov Strictification: Smooth Angular Velocity Observers for Attitude Tracking Control," *Journal of Guidance, Control, and Dynamics*, Vol. 38, No. 3, 2015, pp. 442–451.
doi:10.2514/1.G000779